







## Recurrence of superconductivity in thickness-gradient $\text{La}_{1.81}\text{Ce}_{0.19}\text{CuO}_{4-\delta}$ film

Sijia Tu <sup>1,2</sup>, Jinsong Zhang <sup>1,2</sup>, Zefeng Lin <sup>1,2</sup>, Beiyi Zhu,<sup>1</sup> Qihong Chen <sup>1,2</sup>, Jie Yuan <sup>1,2</sup> and Kui Jin <sup>1,2,3,\*</sup>

<sup>1</sup>Beijing National Laboratory for Condensed Matter Physics, *Institute of Physics, Chinese Academy of Sciences, Beijing 100190, China*

<sup>2</sup>School of Physical Sciences, *University of Chinese Academy of Sciences, Beijing 100049, China*

<sup>3</sup>Songshan Lake Materials Laboratory, *Dongguan, Guangdong 523808, China*



(Received 1 July 2024; accepted 16 August 2024; published 9 September 2024)

We report a systematic study of the thickness effect on the superconductivity of overdoped  $\text{La}_{2-x}\text{Ce}_x\text{CuO}_{4-\delta}$  films. As the film thickness decreases, a recurrence of superconductivity is observed in the  $x = 0.19$  film, while this doping level is commonly expected to show Fermi liquid behavior. The superconducting critical temperatures exhibit a domelike shape with varying thickness. The magnetic susceptibility measurements suggest that the presence of superconductivity in thin films should be filamentary. The combined effect of stress and oxygen in the thickness-gradient films is proposed to comprehend the experimental observations. Our findings provide new perspectives on superconductivity in other systems, such as the hotly debated nickelate superconductors.

DOI: [10.1103/PhysRevMaterials.8.094801](https://doi.org/10.1103/PhysRevMaterials.8.094801)

### I. INTRODUCTION

Recently, thin superconducting films that exhibit anomalous properties such as interface superconductivity [1–4] have attracted intensive attention. Maeda *et al.* [3] fabricated FeSe films on a  $\text{SrTiO}_3$  substrate with a thickness of 7 nm, and the superconducting transition temperature is  $\sim 20$  K, which is much higher than that of bulk FeSe. In TiO films, the thickness- and magnetic-field-tuned superconductor-insulator transition (SIT) manifest quantum Griffiths singularities in this system [5]. The thickness effect, sometimes overlooked but very important, has a close relationship with the superconducting critical transition temperature ( $T_c$ ) [6–9], the lower critical field ( $H_{c1}$ ) [10], the critical current density ( $J_c$ ) [11,12], and other superconducting parameters [13].

For cuprates with layered structures, thickness plays an even more important role in shaping superconducting properties. In the  $\text{YBa}_2\text{Cu}_3\text{O}_y$  (YBCO) system, previous work using magnetron sputtering unveiled a simple relation between  $T_c$  and film thickness  $d$  and found a critical superconducting thickness of  $\sim 1.56$  nm [14]. For optimally doped  $\text{La}_{2-x}\text{Sr}_x\text{CuO}_4$  thin films grown on  $\text{LaSrAlO}_4$  substrates with different crystal orientations, superconductivity emerges at different critical thicknesses [15]. Additionally, as a close relative to cuprates, the infinite-layer nickelate also displays a thickness effect. For example,  $T_c$  of optimally doped  $\text{Nd}_{0.8}\text{Sr}_{0.2}\text{NiO}_2$  thin films increases with increasing thickness [16]. Many studies have reported the effect of thickness on physical properties; However, most of them focused on the optimally doped compounds with the highest  $T_c$ . Overdoped cuprates, which have more dopants but show weakened superconductivity, deserve more attention. In particular, we noticed that Shen *et al.* [17] found the reentrance of superconductivity in heavily overdoped  $\text{La}_{2-x}\text{Sr}_x\text{CuO}_4/\text{LaCuO}_4$

heterostructures, which also intrigued us in the study of the thickness effect in other overdoped cuprates.

The  $\text{La}_{2-x}\text{Ce}_x\text{CuO}_{4-\delta}$  (LCCO) system has the highest  $T_c \sim 30$  K in the electron doped cuprate family, and the optimum doping level is  $x \sim 0.10$  [18–21]. Previous research has indicated that with a decrease in film thickness ( $< 100$  nm), the Hall coefficient of optimally doped  $x \sim 0.10$  LCCO films shifts towards the negative direction and the  $c$ -axis lattice constant increases [22], which can be attributed to the insufficient oxygen reduction during annealing. It is well-known that annealing is essential for the superconductivity in electron-doped cuprates. However, whether it has the same effect on overdoped cuprates is still unclear.

In this work, we fabricated a thickness-gradient LCCO film with the thickness varying from 37.8 to 123.1 nm on a single substrate and the Ce doping is  $x = 0.19$ , which is outside the superconducting dome. Zero resistivity is observed in electrical transport measurement, and  $T_c$  shows a domelike shape as a function of thickness with the highest onset of  $T_c$  ( $T_{c,\text{onset}}$ ) approaching 15 K. The Hall coefficient  $R_H$  remains positive at all measuring temperatures and the Hall carrier density  $n = 1/eR_H$  shows a slight increase with increasing thickness at 2 K. However, the ac magnetic susceptibility measurements show an extremely weak diamagnetic signal across the thickness-gradient film, suggesting the presence of filamentarylike superconductivity [23,24].

### II. METHODS

The thickness-gradient  $\text{La}_{1.81}\text{Ce}_{0.19}\text{CuO}_{4-\delta}$  film was epitaxially grown on a  $10 \times 10 \times 0.5$  mm<sup>3</sup>  $\text{SrTiO}_3(001)$  substrate using laser molecular beam epitaxy (LMBE) with a movable shadow mask. The shadow mask was continuously moving in one direction when the target was ablated, resulting in a film with a linearly varying thickness, as shown in Fig. 1(a). The growing temperature was set at  $\sim 750$  °C and the oxygen partial pressure ( $P(\text{O}_2)$ ) was 0.12 Torr. The fluence and repetition frequency of the KrF excimer laser ( $\lambda = 248$  nm) were set to

\*Contact author: [kuijin@iphy.ac.cn](mailto:kuijin@iphy.ac.cn)

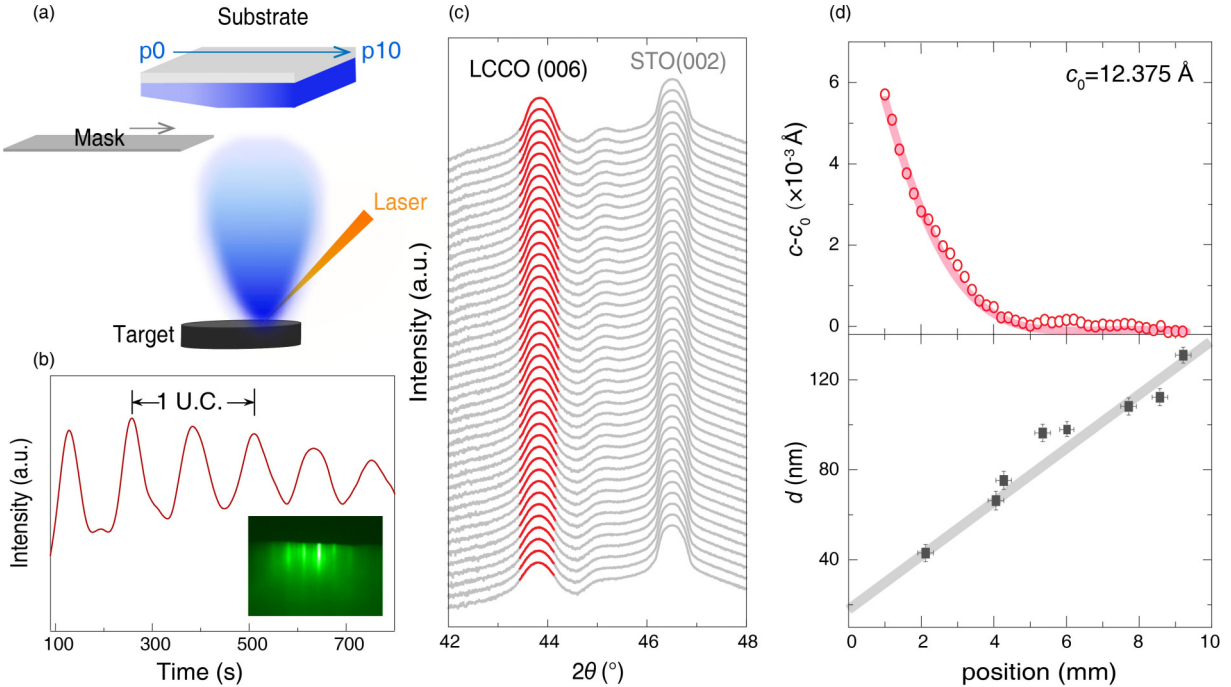


FIG. 1. (a) Schematic illustration of the  $x = 0.19$  LCCO thickness-gradient film grown by pulsed laser deposition with mask technique. (b) The RHEED oscillation curve and diffraction pattern. (c) The micro-region  $\theta/2\theta$  scan along the direction of thickness spread, showing the LCCO (006) and STO (002) Bragg peaks. (d) Upper panels: The position-dependent  $c-c_0$ , where  $c$  is  $c$ -axis lattice parameter and  $c_0 = 12.375 \text{ \AA}$ .  $c_0$  is averaged by ten collected points in the thickest area. Lower panel: The thickness of film at different positions (from p0 to p10, as shown in Fig. 1(a)).

$\sim 2 \text{ J/cm}^2$  and 4 Hz, respectively. Once the deposition process was finished, the film was *in situ* annealed for about 30–60 minutes for better crystallization and oxygen reduction.

The structure information of the film was collected by x-ray diffraction (XRD) using a Rigaku smart lab x-ray diffractometer ( $\text{Cu } K_\alpha$ ;  $\lambda = 0.154 \text{ nm}$ ) with microregion function. Temperature dependence of the electrical resistivity  $\rho$  was measured by the four-probe method in a commercial Physical Properties Measurement System (PPMS). The applied current was fixed at  $50 \text{ }\mu\text{A}$  in the electrical transport measurements. Magnetization was characterized in a magnetic properties measurement system (MPMS) in ac mode. The surface profiler was used to determine the film thicknesses at different positions.

### III. RESULTS

Figure 1(b) displays the time-dependent intensity curve of reflection high-energy electron diffraction (RHEED); the evident oscillating feature suggests that the film grows in a layer-by-layer mode, which can be demonstrated by the striplike RHEED pattern shown in the insert [25]. The interval between two adjacent peaks in the oscillating curve corresponds to a single period of growing one unit cell [25]. Figure 1(c) shows the microregion  $\theta/2\theta$  x-ray diffraction patterns along the thickness-gradient direction, where no apparent impurity peak can be seen. For clarity, the plot is zoomed in between  $42^\circ$  and  $48^\circ$  to show the evolution of two Bragg diffraction peaks, i.e., the (006) peak of the  $\text{La}_{1.81}\text{Ce}_{0.19}\text{CuO}_{4-\delta}$  film and the (002) peak of the  $\text{SrTiO}_3$  substrate, respectively. There is no discernable change in these

two peaks in the whole sample. Based on the microregion XRD measurements, the position-dependent  $c$ -axis lattice parameters can be calculated by the Bragg diffraction formula. The upper panel in Fig. 1(d) provides the evolution of  $c-c_0$  as a function of position with the corresponding variation of thickness shown in the lower panel.  $c_0$  is averaged by ten  $c$  data in the thickest area.

The film was patterned into micro-bridge arrays perpendicular to the thickness-gradient direction for electrical transport measurements [26]. Figure 2(a) exhibits the temperature-dependent resistivity  $\rho(T)$  curves of different regions along the thickness-gradient direction. With the increase of thickness from 37.8 to 123.1 nm (approximately from 30 to 100 unit cells),  $T_{c,\text{onset}}$  exhibits a dome-like behavior. The thickness for the highest  $T_{c,\text{onset}}$  is about 50 nm. The lower panel of Fig. 2(b) gives the evolution of  $\Delta T_c = T_{c,\text{onset}} - T_{c0}$  versus thickness  $d$ .  $T_{c0}$  is defined as the intersection of a line tangent to the steepest part of the resistive transition with the temperature axis. With the increase of  $d$ ,  $\Delta T_c$  decreases quickly and then becomes saturated.

Furthermore, Hall resistivity measurements were carried out on the thickness-gradient film with the magnetic field parallel to the  $c$  axis for  $T = 2 \text{ K}$ ,  $20 \text{ K}$ , and  $100 \text{ K}$ , as seen in Figs. 3(a) and 3(c). Figure 3(d) presents the evolution of the Hall coefficient  $R_H$  with varying thickness  $d$  over a wide range of temperatures.  $R_H$  is always positive but decreases with increasing temperature. The carrier concentration is estimated by the single carrier model  $n = 1/eR_H$ , and the thickness dependence of  $n$  at  $2 \text{ K}$  is shown in Fig. 3(e) by blue dots.  $n$  is independent of  $d$  for  $d < 50 \text{ nm}$ , then gradually increases between  $d \approx 50 \text{ nm}$  and  $100 \text{ nm}$  and

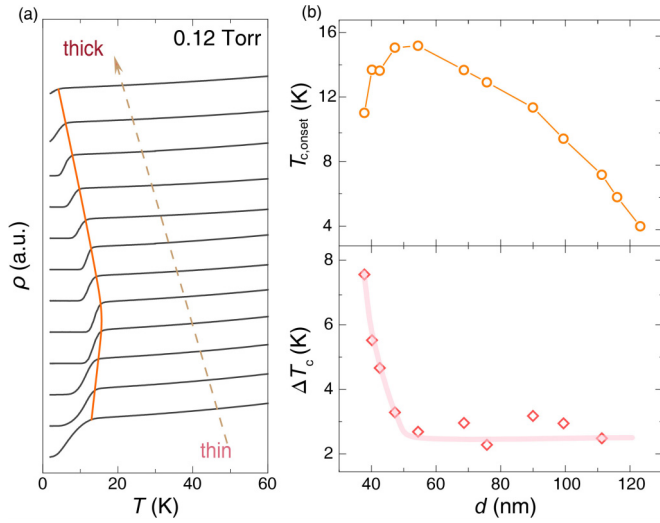


FIG. 2. The micro-region transport properties of the  $x = 0.19$  LCCO thickness-gradient film grown at  $P(\text{O}_2) = 0.12$  Torr. (a) The temperature-dependent resistivities  $\rho(T)$  with the thickness of 37.8 nm, 40.2 nm, 42.6 nm, 47.3 nm, 54.4 nm, 68.6 nm, 75.7 nm, 90.0 nm, 99.4 nm, 111.3 nm, 116.0 nm, and 123.1 nm. (b) The thickness  $d$  dependence of the onset superconducting temperature  $T_{c,\text{onset}}$  and  $\Delta T_c$  ( $\Delta T_c = T_{c,\text{onset}} - T_{c0}$ ).

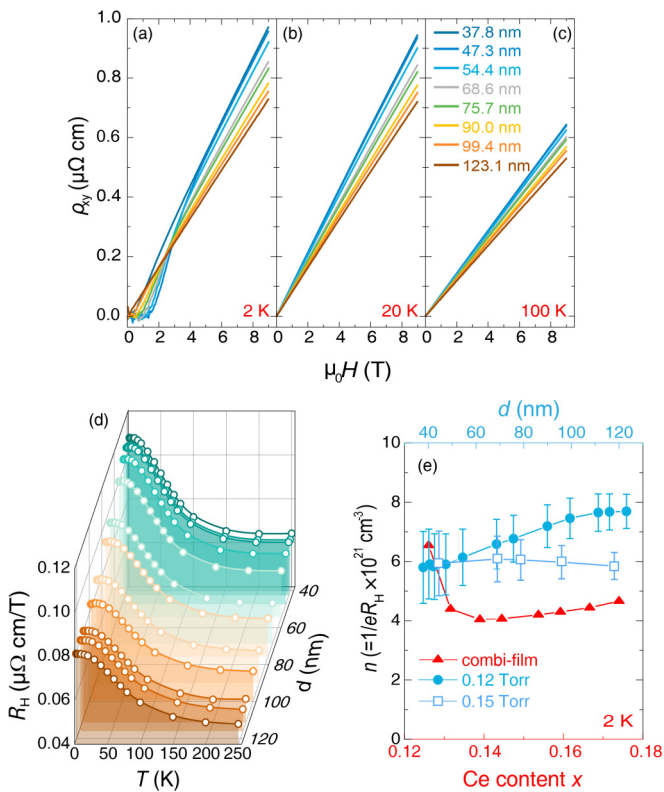


FIG. 3. Evolution of the Hall signal as a function of thickness on the  $x = 0.19$  LCCO thickness-gradient film. The Hall resistivity  $\rho_{xy}$  versus magnetic field  $\mu_0 H$  for different thicknesses at (a) 2 K, (b) 20 K and (c) 100 K. (d) The three-dimensional Hall coefficient  $R_H$  plot at 9 T as functions of temperature and thickness. (e) The carrier density  $n$  of composition spread film (combi-film, red triangles) [26], thickness-gradient film grown at 0.12 Torr (blue dots) and 0.15 Torr (blue squares) at 2 K.

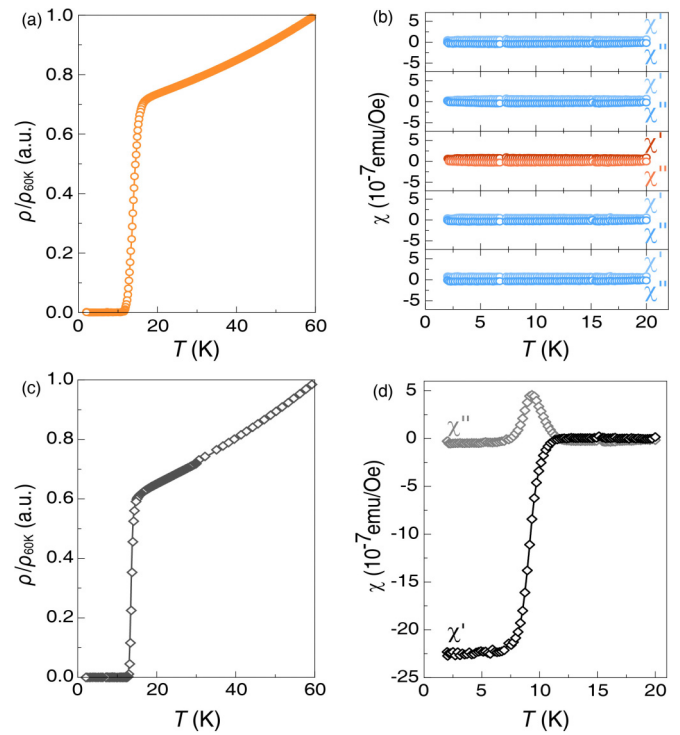


FIG. 4. The normalized resistivity  $\rho$  versus temperature  $T$  for (a) a strip cut from the  $x = 0.19$  thickness-gradient film with the highest  $T_c$  and (c) a Ce content  $x = 0.15$  LCCO film. The ac magnetic susceptibilities of (b) the thickness-gradient film, the orange circles correspond to the strip with the highest  $T_c$  and (d) a Ce content  $x = 0.15$  LCCO film.

finally saturates. In Fig. 3(e), we also plot  $n$  as a function of Ce content  $x$  of LCCO composition-spread film in the range of  $x = 0.126$  to  $0.174$  [26] (represented by red triangles) for comparison. ac magnetic susceptibilities were measured on both a  $x = 0.15$  LCCO film ( $d \sim 100$  nm) and the  $x = 0.19$  LCCO thickness-gradient film. The thickness-gradient film was cut into five strips with the same size ( $\sim 2 \times 6$  mm<sup>2</sup>) for respective measurements. Figure 4(a) shows the normalized resistivity  $\rho$  versus temperature  $T$  for the highest  $T_{c,\text{onset}}$  in the  $x = 0.19$  LCCO thickness-gradient film. The temperature dependence of ac magnetic susceptibilities for all strips is shown in Fig. 4(b), with the middle panel representing the strip for which  $\rho(T)$  is shown in Fig. 4(a). Figures 4(c) and 4(d) present similar measurements for the  $x = 0.15$  LCCO film. Both films have quite similar  $T_c$  and  $T_{c,\text{onset}}$  for the superconducting transition, however, their magnetic susceptibilities are significantly different. The in-plane magnetic susceptibility for the  $x = 0.15$  LCCO film shows diamagnetism of bulk superconductivity. This behavior is absent in the  $x = 0.19$  thickness-gradient film, suggestive of filamentary superconductivity [24].

#### IV. DISCUSSION

The electron-doped LCCO film at  $x = 0.19$ , located outside the superconducting dome, is expected to display Fermi liquid behavior. However, in the thickness-gradient film, it exhibits superconductivity with the highest  $T_{c,\text{onset}}$  of 15 K at the thickness of  $\sim 50$  nm. To figure out this intriguing

phenomenon, the key factors sensitive to thickness need to be carefully examined.

First of all, lattice mismatch between substrate and film is an innegligible issue. The in-plane lattice constant  $a$  of STO, 3.905 Å, is smaller than that of LCCO, 4.01 Å [19,27]. Therefore, the compression stress, which has been reported to lower the  $T_c$  of LCCO film compared to the tensile stress [28], should play a role in the thickness-gradient film. In Fig. 1(d),  $c - c_0$  becomes stable when  $d > 80$  nm, so we take  $d \approx 80$  nm as the critical value for the release of stress in the thickness-gradient film.

Second, the carrier density  $n$  in the thickness-gradient film shows a monotonic behavior across the whole film, rather than a dome-like shape, which indicates that  $n$  is not the key factor for the superconducting dome observed in this thickness-gradient film. Moreover,  $n$  in the thickness-gradient film is larger than that of the LCCO ( $0.13 < x < 0.174$ ) composition-spread film based on our previous study [26]. One may expect that a higher  $T_c$  around 20 K should be observed in the thickness-gradient film, similar to the LCCO film with a Ce content  $x \sim 0.13$ . However, the maximum  $T_c$  of the thickness-gradient film cannot reach  $\sim 20$  K, reinforcing the notion that  $n$  is not the decisive factor for superconductivity.

Tang *et al.* [29] successfully combined ozone annealing and Angle-Resolved Photoemission Spectroscopy (ARPES) measurement on LCCO film with  $x \approx 0.19$ . They found that ozone can change the oxygen content  $4-\delta$  and shift the electron doping level, which means that for nominal  $x = 0.19$  LCCO film, the electron doping level can be tuned into the superconducting dome. In the synthesis of superconducting YBCO [30] and  $\text{Bi}_2\text{Sr}_{2-x}\text{La}_x\text{CuO}_6$  [31], post annealing, which determines  $T_c$ , also involves the oxygen effect. Additionally, for the  $\text{Pr}_{0.88}\text{LaCe}_{0.12}\text{CuO}_{4-\delta}$  single crystal, even though  $T_c$  increases smoothly as oxygen is gradually removed, the signal of bulk superconductivity in specific heat and neutron magnetic resonance can only be detected when  $T_c$  is close to the maximum value [32]. Furthermore, a previous study on overdoped  $\text{Pr}_{2-x}\text{Ce}_x\text{CuO}_4$  (PCCO) films found that altering annealing oxygen pressures can result in behaviors that vary from nonsuperconducting in underdopedlike states to superconducting in overdoped states, the accumulation of oxygen vacancies in the  $\text{CuO}_2$  plane is suggested to be responsible for the observed superconductivity [33]. These observations highlight the complex role of oxygen in cuprates, particularly for bulk superconductivity. All these factors prompt us to examine the oxygen effect in the thickness-gradient film, therefore, the other overdoped  $x = 0.19$  LCCO thickness-gradient film grown at a higher oxygen partial pressure  $P(\text{O}_2) = 0.15$  Torr was also investigated. Figure 5 displays the  $\rho(T)$  curves and the Hall carrier density  $n$  is shown in Fig. 3(e) by blue squares. It is interesting to see that the film grown at 0.15 Torr shows weaker superconductivity than that at 0.12 Torr. The highest  $T_{c,\text{onset}}$  is lowered by  $\sim 5$  K and the corresponding thickness shifts from 50 nm to 80 nm. The Hall carrier density  $n$  at 2 K for the film grown at 0.15 Torr is smaller and roughly constant across the whole chip.

Taking into account all the factors mentioned above, speculations about the superconductivity in the  $x = 0.19$  LCCO thickness-gradient film grown at 0.12 Torr are given as follows. For this thickness-gradient film, the initial increase of

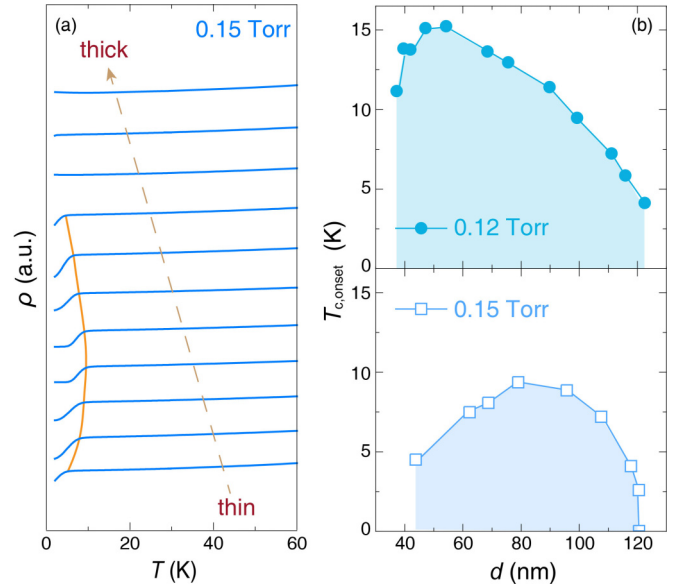


FIG. 5. (a) The temperature-dependent resistivities of  $x = 0.19$  LCCO thickness-gradient film grown at oxygen pressure  $P(\text{O}_2) = 0.15$  Torr, with the thickness of 44.4 nm, 61.6 nm, 68.9 nm, 78.8 nm, 95.9 nm, 108.2 nm, 113.1 nm, 118.0 nm, 120.5 nm, 122.9 nm, and 127.8 nm. (b) The thickness-dependent  $T_{c,\text{onset}}$  for the thickness-gradient films deposited under different oxygen pressures, 0.12 Torr (upper panel) and 0.15 Torr (lower panel), respectively.

$T_c$ , corresponding to the thickness of less than 50 nm, probably originates from the competition between compression stress and oxygen vacancies. References [34–36] indicate that thinner films are likely to have a higher density of oxygen vacancies under the same annealing conditions. Consequently, in our thickness-gradient film, as the thickness decreases, an increase in oxygen vacancies can be expected, potentially leading to improved superconductivity, as proposed by references [33,37,38]. It's worth noting that compression stress may counteract this effect. As a result,  $T_c$  decreases when the thickness is smaller than 50 nm, where the lattice strain effect dominates. When  $d \approx 50$  nm, these two factors reach a balance, resulting in the highest  $T_c$ , in agreement with the fact that  $\Delta T_c$  levels off once the thickness  $d$  exceeds 50 nm. The initial decrease in  $\Delta T_c$  manifests the interplay between the oxygen vacancy effect and the stress effect, which diminishes rapidly with increasing film thickness. When  $d > 50$  nm, both the stress effect and the oxygen vacancy effect weaken, and the dominant role of oxygen vacancies results in decreases of  $T_c$ , and  $\Delta T_c$  remains constant. In Fig. 3(e),  $n$  of the thickness-gradient films and the composition-spread film were plotted in the same figure to demonstrate the different impacts of Ce doping and oxygen vacancies. For the thickness-gradient films with a nominal Ce doping level of  $x = 0.19$ , the carrier density of the film grown at a higher oxygen pressure  $P(\text{O}_2) = 0.15$  Torr is closer to that of the  $x = 0.19$  point of the composition-spread film. This suggests that the property of the  $P(\text{O}_2) = 0.15$  Torr film should be expected to reside closer to the composition-spread film, which is not superconducting at  $x = 0.19$ . The primary difference between the two thickness-gradient films is the density of oxygen vacancies in the  $\text{CuO}_2$  plane. In this case, the vacancies tend to localize

the additional electrons on the nearby copper site, unlike the apical oxygen scenario, where the reduction in oxygen content has a similar effect to cerium doping. As a result,  $n$  would have a complex dependence on the oxygen vacancies. Besides, our research indicates that the oxygen vacancies discussed are local, supported by the results of magnetic susceptibility measurements. Therefore, finding a direct correlation between carrier density and superconductivity is challenging in this work, as it is affected by many factors.

In the present work, it is still hard to pin down the cause of filamentary superconductivity, yet the oxygen effect is certainly involved. Besides, the phase separation with percolative superconducting puddles offers a possibility for inhomogeneity in cuprates [39–41], which cannot be completely ruled out here. Since there is no obvious diamagnetism signal in the susceptibility measurement, further experiments with spatial resolution are designated to map the superconductivity in the thinner film, including the scale of inhomogeneities [42]. Focusing on the superconductivity phenomenon, the highest  $T_{c,\text{onset}}$  in the thickness-gradient film is about 15 K, which is similar to the  $T_c$  value of  $x = 0.15$  LCCO films. It appears difficult to achieve a higher  $T_c$  exceeding 15 K, which may be due to the Fermi surface reconstruction (FSR) phenomenon that occurs in the LCCO system when  $x = 0.14$  [43]. This is a plausible outcome, given the different effects of oxygen and cerium doping on superconductivity [33,44]. An alternative explanation is that  $T_c$  is constrained from further elevation due to unavoidable stress effects.

## V. CONCLUSION

We have fabricated a  $x = 0.19$  thickness-gradient LCCO film to investigate the thickness effect on overdoped cuprates.

Surprisingly, instead of exhibiting metallic behavior,  $T_c$  of the thickness-gradient film exhibits a dome-like behavior with the increase of thickness. The initial increase in  $T_c$  is the result of the competition between compressive stress, which tends to decrease  $T_c$ , and oxygen vacancies, which increase  $T_c$ . However, with a further increase in thickness, the stress effect disappears, and the reduction in  $T_c$  is attributed to the dominant role of oxygen vacancies. It is important to note that the oxygen vacancies mentioned here may be local and the superconductivity observed in the overdoped thickness-gradient film is filamentary-like, as evidenced by the lack of signal in Meissner effect measurements. Our research on the thickness effect in overdoped cuprates provides a fresh perspective on comprehending superconductivity, not only in cuprates but also in other layered superconducting structures.

## ACKNOWLEDGMENTS

This work was supported by the National Natural Science Foundation of China (12225412, 12374141, 12204333, 12274439, 11834016, 11927808, 11961141008, U23A6015), the National Key Basic Research Program of China (2021YFA0718700, 2022YFA1403900, 2022YFA1603903, 2022YFA1403000), the Strategic Priority Research Program (B) of Chinese Academy of Sciences (XDB25000000, XDB33000000), the Beijing Nova Program of Science and Technology (20220484014), CAS Project for Young Scientists in Basic Research (2022YSBR-048), and the Key-Area Research and Development Program of Guangdong Province (Grant No. 2020B0101340002).

- 
- [1] J. Wu, O. Pelleg, G. Logvenov, A. T Bollinger, Y.-J. Sun, G. S. Boebinger, M. Vanević, Z. Radović, and I. Božović, *Nat. Mater.* **12**, 877 (2013).
  - [2] J. J. Lee, F. T. Schmitt, R. G. Moore, S. Johnston, Y.-T. Cui, W. Li, M. Yi, Z. K. Liu, M. Hashimoto, and Y. Zhang, *Nature (London)* **515**, 245 (2014).
  - [3] T. Kobayashi, H. Ogawa, F. Nabeshima, and A. Maeda, *Supercond. Sci. Technol.* **35**, 07LT01 (2022).
  - [4] M. Hosoda, C. Bell, Y. Hikita, and H. Y. Hwang, *Appl. Phys. Lett.* **102**, 91601 (2013).
  - [5] C. Zhang, Y. Fan, Q. Chen, T. Wang, X. Liu, Q. Li, Y. Yin, and X. Li, *Npg Asia Mater.* **11**, 76 (2019).
  - [6] D. Costanzo, S. Jo, H. Berger, and A. F Morpurgo, *Nat. Nanotechnol.* **11**, 339 (2016).
  - [7] D. T. Harris, N. Campbell, R. Uecker, M. Brützam, D. G. Schlom, A. Levchenko, M. S. Rzchowski, and C.-B. Eom, *Phys. Rev. Mater.* **2**, 041801(R) (2018).
  - [8] N. Marković, C. Christiansen, and A. M. Goldman, *Phys. Rev. Lett.* **81**, 5217 (1998).
  - [9] R. G. Goodrich, P. W. Adams, D. H. Lowndes, and D. P. Norton, *Phys. Rev. B* **56**, R14299 (1997).
  - [10] T. Tan, M. A. Wolak, N. Acharya, A. Krick, A. C. Lang, J. Sloppy, M. L. Taheri, L. Civale, K. Chen, and X. X. Xi, *APL Mater.* **3**, 41101 (2015).
  - [11] E. F. Talantsev and J. L. Tallon, *Nat. Commun.* **6**, 7820 (2015).
  - [12] E. Polturak, G. Koren, D. Cohen, E. Aharoni, and G. Deutscher, *Phys. Rev. Lett.* **67**, 3038 (1991).
  - [13] J. Shiogai, T. Miyakawa, Y. Ito, T. Nojima, and A. Tsukazaki, *Phys. Rev. B* **95**, 115101 (2017).
  - [14] W. H. Tang, C. Y. Ng, C. Y. Yau, and J. Gao, *Supercond. Sci. Technol.* **13**, 580 (2000).
  - [15] H. Sato, *Physica C (Amsterdam, Neth.)* **468**, 991 (2008).
  - [16] S. W. Zeng, X. M. Yin, C. J. Li, L. E. Chow, C. S. Tang, K. Han, Z. Huang, Y. Cao, D. Y. Wan, and Z. T. Zhang, *Nat. Commun.* **13**, 743 (2022).
  - [17] J. Y. Shen, C. Y. Shi, Z. M. Pan, L. L. Ju, M. D. Dong, G. F. Chen, Y. C. Zhang, J. K. Yuan, C. J. Wu, and Y. W. Xie, *Nat. Commun.* **14**, 7290 (2023).
  - [18] K. Jin, N. P. Butch, K. Kirshenbaum, J. Paglione, and R. L. Greene, *Nature (London)* **476**, 73 (2011).
  - [19] M. Naito, S. Karimoto, and A. Tsukada, *Supercond. Sci. Technol.* **15**, 1663 (2002).
  - [20] A. Sawa, M. Kawasaki, H. Takagi, and Y. Tokura, *Phys. Rev. B* **66**, 014531 (2002).
  - [21] Y. Krockenberger, J. Kurian, A. Winkler, A. Tsukada, M. Naito, and L. Alff, *Phys. Rev. B* **77**, 060505(R) (2008).
  - [22] B. X. Wu, K. Jin, J. Yuan, H. B. Wang, T. Hatano, B. R. Zhao, and B. Y. Zhu, *Supercond. Sci. Technol.* **22**, 85004 (2009).

- [23] S. W. Hsu, S. Y. Tsaur, and H. C. Ku, *Phys. Rev. B* **38**, 856 (1988).
- [24] S. A. Shaheen, N. Jisrawi, Y. H. Lee, Y. Z. Zhang, M. Croft, W. L. McLean, H. Zhen, L. Rebelsky, and S. Horn, *Phys. Rev. B* **36**, 7214 (1987).
- [25] T. Terashima, Y. Bando, K. Iijima, K. Yamamoto, K. Hirata, K. Hayashi, K. Kamigaki, and H. Terauchi, *Phys. Rev. Lett.* **65**, 2684 (1990).
- [26] J. Yuan, Q. Chen, K. Jiang, Z. Feng, Z. Lin, H. Yu, G. He, J. Zhang, X. Jiang, and X. Zhang, *Nature (London)* **602**, 431 (2022).
- [27] T. Greibe, M. Hepp, and M. Naito, *Physica C* **372**, 1082 (2002).
- [28] J. Yuan, S. J. Zhu, K. Jin, H. Wu, B. Xu, X. G. Qiu, and B. R. Zhao, *Physica C: Supercond. Applic.* **468**, 1876 (2008).
- [29] C. Y. Tang, Z. F. Lin, J. X. Zhang, X. C. Guo, J. Y. Guan, S. Y. Gao, Z. C. Rao, J. Zhao, Y. B. Huang, and T. Qian, *Phys. Rev. B* **104**, 155125 (2021).
- [30] Z. Mori, T. Doi, and Y. Hakuraku, *J. Appl. Phys.* **107**, 23903 (2010).
- [31] C. Cancellieri, P. H. Lin, D. Ariosa, and D. Pavuna, *J. Phys.: Condens. Matter* **19**, 246214 (2007).
- [32] S. Li, S. Chi, J. Zhao, H.-H. Wen, M. B. Stone, J. W. Lynn, and P. Dai, *Phys. Rev. B* **78**, 014520 (2008).
- [33] J. Gauthier, S. Gagné, J. Renaud, M.-È Gosselin, P. Fournier, and P. Richard, *Phys. Rev. B* **75**, 024424 (2007).
- [34] L. Dai, G. Niu, J. Zhao, Y. Xue, R. Luo, B. Chen, R. An, Y. Sun, B. Feng, and S. Ding, *J. Appl. Phys.* **129**, 45302 (2021).
- [35] H.-B. Jang, J. S. Lim, and C.-H. Yang, *Sci. Rep.* **10**, 3236 (2020).
- [36] F. Zheng, G. Logvenov, I. Bozovic, Y. Zhu, and J. He, *Phys. Rev. B* **89**, 184509 (2014).
- [37] P. Richard, G. Riou, I. Hetel, S. Jandl, M. Poirier, and P. Fournier, *Phys. Rev. B* **70**, 064513 (2004).
- [38] G. Riou, P. Richard, S. Jandl, M. Poirier, P. Fournier, V. Nekvasil, S. N. Barilo, and L. A. Kurnevich, *Phys. Rev. B* **69**, 024511 (2004).
- [39] Y. Koike, T. Adachi, Y. Tanabe, K. Omori, T. Noji, and H. Sato, *J. Phys.: Conf. Ser.* **108**, 012003 (2008).
- [40] Y. Tanabe, T. Adachi, K. Omori, H. Sato, and Y. Koike, *Physica C (Amsterdam, Neth.)* **460**, 376 (2007).
- [41] Y. J. Uemura, *Physica C: Supercond. Applic.* **282**, 194 (1997).
- [42] D. N. Basov, R. D. Averitt, D. van der Marel, M. Dressel, and K. Haule, *Rev. Mod. Phys.* **83**, 471 (2011).
- [43] T. Sarkar, P. R. Mandal, J. S. Higgins, Y. Zhao, H. Yu, K. Jin, and R. L. Greene, *Phys. Rev. B* **96**, 155449 (2017).
- [44] J. S. Higgins, Y. Dagan, M. C. Barr, B. D. Weaver, and R. L. Greene, *Phys. Rev. B* **73**, 104510 (2006).